AN EDGE-BASED SMOOTHED FINITE ELEMENT FOR BUCKLING ANALYSIS OF FUNCTIONALLY GRADED MATERIAL VARIABLE-THICKNESS PLATES

Tran Trung Thanh[1]**, Tran Van Ke**[1]**, Pham Quoc Hoa**[2]**,
Tran The Van**[2]**, Nguyen Thoi Trung**[3,*]
[1]*Le Quy Don Technical University, Hanoi, Vietnam*
[2]*Tran Dai Nghia University, Ho Chi Minh City, Vietnam*
[3]*Ton Duc Thang University, Ho Chi Minh City, Vietnam*
[*]E-mail: nguyenthoitrung@tdtu.edu.vn

Abstract. The paper aims to extend the ES-MITC3 element, which is an integration of the edge-based smoothed finite element method (ES-FEM) with the mixed interpolation of tensorial components technique for the three-node triangular element (MITC3 element), for the buckling analysis of the FGM variable-thickness plates subjected to mechanical loads. The proposed ES-MITC3 element is performed to eliminate the shear locking phenomenon and to enhance the accuracy of the existing MITC3 element. In the ES-MITC3 element, the stiffness matrices are obtained by using the strain smoothing technique over the smoothing domains formed by two adjacent MITC3 triangular elements sharing the same edge. The numerical results demonstrated that the proposed method is reliable and more accurate than some other published solutions in the literature. The influences of some geometric parameters, material properties on the stability of FGM variable-thickness plates are examined in detail.

Keywords: buckling analysis, critical load, variable thickness plate, edge-based finite element method, ES-MITC3.

1. INTRODUCTION

The functionally graded materials (FGMs) can change the material properties gradually, continuously, and smoothly in different directions. Therefore, the delamination in laminated composites can be eliminated in these materials. They are made of two components, mainly metal with high toughness and ceramic with outstanding heat and corrosive resistance properties. Due to such excellent properties, they are applied in various high-tech industries such as automotive, nuclear, civil engineering, and aerospace. There have been many studies on the mechanical behavior of FGM structures including the buckling problem. Some typical studies can be summarized as follows. Ramu et

al. [1] studied the stability of FGM under uniaxial and biaxial compression load using the finite element method (FEM) based on classical plate theory (CPT). Rohit et al. [2] used third-order shear deformation theories (TSDT) to analyze the buckling of the simple supported FGM plates under uniaxial load. Wu et al. [3] studied the stability of FGM plates subjected to thermal and mechanical loads using FSDT. Javaheri et al. [4] based on the analytical method (AM) for the stability analysis of FGM plates subjected to inplane compressive load. Zenkour [5] calculated the free vibration and buckling of FGM constant-thickness sandwich plates. Shariat et al. [6] studied the buckling of thick FGM plate by AM. Thai et al. [7] used an efficient and simple refined theory for buckling analysis of FGM plates. Reddy [8] combined an analytical method and TSDT to analyze the buckling of the FGM plate. Thinh et al. [9] proposed an eight unknown higher-order shear deformation theory for vibration and buckling analysis of constant-thickness FGM plates.

Variable-thickness structures are extensively used in many types of highperformance surfaces like aircraft, civil engineering, and other engineering fields. Using these structures will help adjust the weight of structural, and hence help maximize the capacity of the material. For example, Thang et al. [10] investigated the effects of variablethickness on buckling and post-buckling of imperfect sigmoid FGM plates on elastic foundation (EF) subjected to compressive loading. Eisenberger et al. [11] investigated the buckling of variable-thickness thin isotropic plates by using the extended Kantorovich method. Naei et al. [12] analyzed the buckling of the FGM variable-thickness circularplate using FEM. Jalali et al. [13] investigated thermal buckling of the FGM nonuniformthickness circular sandwich plates employed the pseudo-spectral method. Alipour and co-workers used semi-analytical to studied buckling of heterogeneous variable-thickness viscoelastic circular-plates lying on the EF [14], and variable-thickness bi-directional FGM circular-plates placed on nonuniform-EF [15]. Alinaghizadeh et al. [16] applied the generalized differential quadrature (GDQ) method for buckling analysis of variable-thickness radially FGM annular sector plates located on two parameters EF. Bouguenina et al. [17] conducted analyses of FGM variable-thickness plates under thermal loads using finite difference method. Benlahcen et al. [18] employed an analytical solution to examine buckling of simply supported FGM plates with parabolic-concave thickness variation. Minh and Duc [19] investigated the effect of cracks on the stability of the FGM variablethickness plates using TSDT and phase-field theory. In addition, Zenkour [20] presented the hygrothermal mechanical bending of variable-thickness plates using the AM. Allam et al. [21] investigated thermoelastic stresses in FG variable-thickness rotating annular disks using infinitesimal theory. Thien et al. [22] developed the isogeometric analysis (IGA) to analyze the buckling of non-uniform thickness nanoplates resting on the EF.

To improve the convergence and accuracy for classical triangular elements, the origin MITC3 element [23] is proposed to combine with the ES-FEM [24] to give the so-called ES-MITC3 element [25–30]. In the formulation of the ES-MITC3 element, the system stiffness matrix is employed using strains smoothed over the smoothing domains associated with the edges of the triangular elements. The numerical results of the present study demonstrated that the ES-MITC3 element has the following superior properties: (1) the ES-MITC3 element can avoid the transverse shear locking phenomenon even with the

ratio of the thickness to the length of the structures reach 10^{-8} (readers can see detail in Ref. [25]; (2) the ES-MITC3 element has higher accuracy than the existing triangular elements such as MITC3 element [23], DSG3 element [31] and CS-DSG3 element [32]; and is a good competitor with the MITC4 element [33].

According to the best of authors' knowledge, the stability of FGM variable-thickness plates using the ES-MITC3 element has not yet been studied. Therefore, this paper aims to extend the ES-MITC3 element for the buckling analysis of FGM variable-thickness plates. The formulation is based on the FSDT due to its simplicity and computational efficiency. The accuracy and reliability of the present approach are verified by comparing the present numerical results with those of other available methods. Finally, the influence of geometrical parameters, and material properties on the buckling of FGM plates are fully studied.

2. THEORETICAL FORMULATION

2.1. FGM material

The FGM is made up of two components: ceramic and metal. The mechanical properties of FGM are assumed to vary smoothly through the thickness of plates as follows [6]

$$P\left(z\right) = \left(P_c - P_m\right) V_c\left(z\right) + P_m, \tag{1}$$

$$V_c(z) = \left(\frac{z}{h(x,y)} + 0.5\right)^p \text{ with } z \in \left[-\frac{h\left(x,y\right)}{2}; \frac{h\left(x,y\right)}{2}\right], \tag{2}$$

in which $P\left(z\right)$ represents for Young's modulus $E(z)$, Poisson's ratio $v(z)$; subscripts m and c denotes the metal and ceramic constituents; $V_c(z)$ is the volume fraction of ceramic which according to a power-law function with p is the power-law index. The value of p equals to 0 and $+\infty$ represents a fully ceramic and fully metal plate, respectively. Note that, the thickness of plate is different at various positions on the plate and depends on the law of thickness variation (h is the function of x- and y-variables).

2.2. Mindlin's plate theory

According to Mindlin's plate theory, the displacement field of the plate is given by [1]

$$\begin{cases} u\left(x,y,z\right) = u_0\left(x,y\right) + z\theta_x\left(x,y\right) \\ v\left(x,y,z\right) = v_0\left(x,y\right) + z\theta_y\left(x,y\right) \\ w\left(x,y,z\right) = w_0\left(x,y\right) \end{cases} \tag{3}$$

in which $u, v, w, \theta_x, \theta_y$ are five unknown displacements of the mid-surface of the plate.

The strain field can be expressed as follows

$$\varepsilon = \begin{Bmatrix} \varepsilon_x \\ \varepsilon_y \\ \varepsilon_{xy} \\ \gamma_{xz} \\ \gamma_{yz} \end{Bmatrix} = \begin{Bmatrix} u_{,x} \\ v_{,y} \\ u_{,y} + v_{,x} \\ w_{,x} + u_{,z} \\ w_{,y} + v_{,z} \end{Bmatrix} = \begin{Bmatrix} u_{0,x} \\ v_{0,y} \\ u_{0,y} + v_{0,x} \\ v_{0.x} + \theta_x \\ w_{0,y} + \theta_y \end{Bmatrix} + z \begin{Bmatrix} \theta_{x,x} \\ \theta_{y,y} \\ \theta_{x,y} + \theta_{y,x} \\ 0 \\ 0 \end{Bmatrix}. \tag{4}$$

Eq. (3) may be written by

$$= \left\{ \begin{array}{c} \varepsilon_1 \\ \varepsilon_2 \end{array} \right\} = \left\{ \begin{array}{c} \varepsilon_m + z\boldsymbol{\kappa} \\ \gamma \end{array} \right\}. \tag{5}$$

From Hooke's law, the linear stress-strain relations can be determined by a formulation

$$\left\{ \begin{array}{c} \sigma_x \\ \sigma_y \\ \sigma_{xy} \\ \tau_{xz} \\ \tau_{yz} \end{array} \right\} = \left[\begin{array}{ccccc} Q_{11} & Q_{12} & 0 & 0 & 0 \\ Q_{21} & Q_{22} & 0 & 0 & 0 \\ 0 & 0 & Q_{66} & 0 & 0 \\ 0 & 0 & 0 & Q_{55} & 0 \\ 0 & 0 & 0 & 0 & Q_{44} \end{array} \right] \left\{ \begin{array}{c} \varepsilon_x \\ \varepsilon_y \\ \varepsilon_{xy} \\ \gamma_{xz} \\ \gamma_{yz} \end{array} \right\}, \tag{6}$$

in which

$$Q_{11} = Q_{22} = \frac{E(z)}{1 - v(z)^2}, \ Q_{12} = Q_{21} = \frac{v(z)E(z)}{1 - v(z)^2}, \ Q_{44} = Q_{55} = Q_{66} = \frac{E(z)}{2(1 + v(z))}. \tag{7}$$

The force and moment resultants are obtained as follows [30]

$$\left\{ N_x \ N_y \ N_{xy} \right\}^T = \boldsymbol{A}\varepsilon_m + \boldsymbol{B}\boldsymbol{\kappa}, \tag{8a}$$

$$\left\{ M_x \ M_y \ M_{xy} \right\}^T = \boldsymbol{B}\varepsilon_m + \boldsymbol{C}\boldsymbol{\kappa}, \tag{8b}$$

$$\left\{ Q_{xz} \ Q_{yz} \right\}^T = \boldsymbol{A}^s\gamma, \tag{8c}$$

with

$$(\boldsymbol{A}, \boldsymbol{B}, \boldsymbol{C}) = \int_{-h(x,y)/2}^{h(x,y)/2} \left[\begin{array}{ccc} Q_{11} & Q_{12} & 0 \\ Q_{21} & Q_{22} & 0 \\ 0 & 0 & Q_{66} \end{array} \right] \left(1, z, z^2\right) dz, \tag{9}$$

$$\boldsymbol{A}^s = \int_{-h(x,y)/2}^{h(x,y)/2} \left[\begin{array}{cc} Q_{55} & 0 \\ 0 & Q_{44} \end{array} \right] dz. \tag{10}$$

It should be noted that compared to uniform thickness plates, all the matrices in Eqs. (9) and (10) depend on the law of thickness variation and thus the limits of integrations also depend on the position of points on plates.

2.3. Finite element formulation for buckling analysis of FGM variable-thickness plates

The bounded domain Ω of the FGM plate is discretized into n^e three-node triangular elements with n^n nodes such that $\psi \approx \sum_{e=1}^{n^e} \psi_e$ and $\psi_i \cap \psi_j = \varnothing, i \neq j$. Then the generalized displacements at any point $\boldsymbol{u}^e = \left[u_j^e, v_j^e, w_j^e, \theta_{xj}^e, \theta_{yj}^e \right]^T$ of the element ψ_e can be approximated as [23]

$$\boldsymbol{u}^e(\boldsymbol{x}) = \sum_{j=1}^{n^{ne}} \left[\begin{array}{ccccc} N_I(\boldsymbol{x}) & 0 & 0 & 0 & 0 \\ 0 & N_I(\boldsymbol{x}) & 0 & 0 & 0 \\ 0 & 0 & N_I(\boldsymbol{x}) & 0 & 0 \\ 0 & 0 & 0 & N_I(\boldsymbol{x}) & 0 \\ 0 & 0 & 0 & 0 & N_I(\boldsymbol{x}) \end{array} \right] \boldsymbol{d}_j^e = \sum_{j=1}^{n^{ne}} \boldsymbol{N}(\boldsymbol{x}) \boldsymbol{d}_j^e, \tag{11}$$

where n^{ne} is the number of nodes of ψ_e; $N(x)$ is the shape function matrix; and $d_j^e = \left[u_j^e, v_j^e, w_j^e, \theta_{xj}^e, \theta_{yj}^e \right]^T$ are the nodal degrees of freedom (DOF) associated with the jth node of ψ_e.

The membrane bending strains of MITC3 element can be expressed in the matrix form as follows [23]

$$\varepsilon_m^e = \begin{bmatrix} B_{m1}^e & B_{m2}^e & B_{m3}^e \end{bmatrix} d^e = B_m^e d^e, \tag{12a}$$

$$\kappa^e = \begin{bmatrix} B_{b1}^e & B_{b2}^e & B_{b3}^e \end{bmatrix} d^e = B_b^e d^e. \tag{12b}$$

The smoothing domains ψ^k is constructed based on the edges of the triangular elements such that $\psi = \cup_{k=1}^{nk} \psi^k$ and $\psi_i^k \cap \psi_j^k = \varnothing$ for $i \neq j$. An edge-based smoothing domain ψ^k for the inner edge k is formed by connecting two end-nodes of the edge to the centroids of adjacent triangular MITC3 elements as shown in Fig. 1.
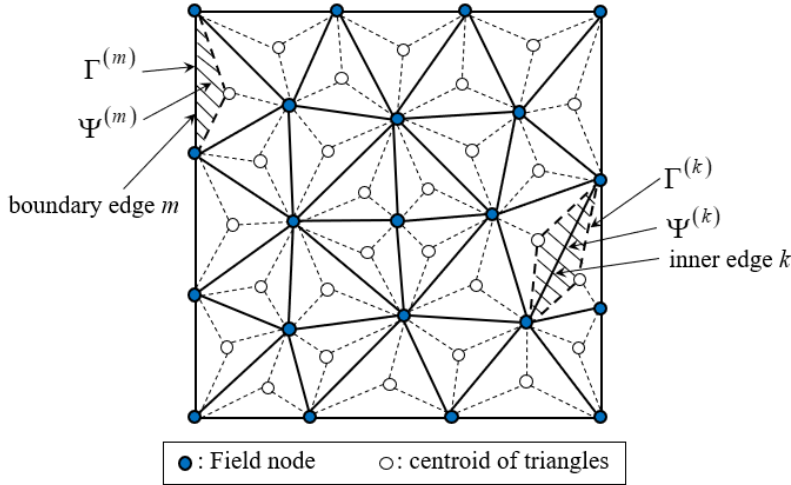
Fig. 1. The smoothing domain ψ^k is formed by triangular elements

Applying the edge-based smooth technique [24], the smoothed membrane, bending and shear strain $\tilde{\varepsilon}_m^k, \tilde{\kappa}^k, \tilde{\gamma}^k$ over the smoothing domain ψ^k can be created by

$$\tilde{\varepsilon}_m^k = \int_{\psi^k} \varepsilon_m \Phi^k(x) \, d\psi, \tag{13a}$$

$$\tilde{\kappa}^k = \int_{\psi^k} \kappa \Phi^k(x) \, d\psi, \tag{13b}$$

$$\tilde{\gamma}^k = \int_{\psi^k} \gamma \Phi^k(x) \, d\psi, \tag{13c}$$

where ε_m, κ and γ the compatible membrane, bending and the shear strains, respectively; $\Phi^k(x)$ is a given smoothing function that satisfies at least the unity property $\int_{\psi^k} \Phi^k(x) \, d\psi = 1$.

In this study, we use the constant smoothing function [24]

$$\Phi^k(x) = \begin{cases} \dfrac{1}{A^k}, & x \in \psi^k \\ 0, & x \notin \psi^k \end{cases} \tag{14}$$

in which A^k is the area of the smoothing domain ψ^k and is given by

$$A^k = \int_{\psi^k} \mathrm{d}\psi = \frac{1}{3} \sum_{i=1}^{n^{ek}} A^i, \tag{15}$$

where n^{ek} is the number of the adjacent triangular elements in the smoothing domain ψ^k; and A^i is the area of the ith triangular element attached to the edge k.

The stiffness matrix of the FGM plate using the ES-MITC3 element is assembled by [24]

$$\tilde{K}_p = \sum_{k=1}^{n_{sh}^k} \tilde{K}_e^k, \tag{16}$$

where $\widetilde{K}_e^k$ is the ES-MITC3 element stiffness matrix of the smoothing domain ψ^k and given by

$$\tilde{K}_e^k = \int_{\psi^k} \left(\tilde{B}^{kT} \begin{bmatrix} A & B \\ B & C \end{bmatrix} \tilde{B}^k + \tilde{B}_s^{kT} A^s \tilde{B}_s^k \right) \mathrm{d}\psi = \tilde{B}^{kT} \begin{bmatrix} A & B \\ B & C \end{bmatrix} \tilde{B}^k A^k + \tilde{B}_s^{kT} A^s \tilde{B}_s^k A^k, \tag{17}$$

in which

$$\tilde{B}^{kT} = \begin{bmatrix} \tilde{B}_{mj}^k & \tilde{B}_{bj}^k \end{bmatrix}, \tag{18}$$

and the strain-displacement matrices are presented in detail in [30].

The geometric stiffness matrix of the FGM plate using the ES-MITC3 element is determined by [28]

$$\tilde{K}_g = \sum_{k=1}^{n_{sh}^k} \tilde{K}_g^{ek} \text{ with } \tilde{K}_g^e = \int_{\psi^k} \left(\tilde{Y}_i^T \bar{N} \tilde{Y}_i \right) \mathrm{d}\psi, \tag{19}$$

where

$$\overline{N} = \begin{bmatrix} \overline{N}_x & \overline{N}_{xy} \\ \overline{N}_{xy} & \overline{N}_y \end{bmatrix}, \tag{20}$$

with

$$\left(\overline{N}_x, \overline{N}_y, \overline{N}_{xy} \right) = \int_{-h(x,y)}^{h(x,y)} \left(\sigma_x, \sigma_y, \sigma_{xy} \right) \mathrm{d}z, \tag{21}$$

and $\tilde{Y}_i$ is presented in [28]. It is noted that the integrations in Eq. (21) also depend on the law of thickness variation, therefore the limits of integrations will depend on the position of points on plates.

Apply the principle of minimum total potential energy, the stability problem involves the solution of the following eigen problem in which P_{cr} is the critical load

$$\left| \tilde{K}_p + P_{cr} \tilde{K}_g \right| = 0. \tag{22}$$

3. CONVERGENCE AND ACCURACY OF THE PROPOSED METHOD

In order to evaluate the convergence and accuracy of the proposed method, the authors consider the following two examples:

Example 1. Firstly, we consider a fully clamped (CCCC) FGM constant-thickness plate with material properties given by the metal (Al) $E_m = 70\,\text{GPa}$, $v_m = 0.3$ and ceramic (Al$_2$O$_3$) $E_c = 380\,\text{GPa}$, $v_c = 0.3$. The non-dimensional critical load P^*_{cr} of FGM plates with different mesh-size are listed in Table 1. It can be seen that, in all cases, the results by the ES-MITC3 element converge faster and are more accurate than those by the MITC3 element. Specifically, at the 18×18 mesh-size, the ES-MITC3 element gives

Table 1. The convergence of mesh-size of non-dimensional critical load $P^*_{cr} = P_{cr}b^2/E_c h_0^3$ of CCCC square FGM plates

a/h	p	Mesh size	ES-MITC3	Error (%)	MITC3	Error (%)	Wu [3]
		12×12	4.6212	0.12	4.6265	0.23	
		14×14	4.6185	0.06	4.6210	0.11	
100	1	16×16	4.6167	0.02	4.6194	0.08	4.6158
		18×18	4.6160	0.01	4.6180	0.05	
		20×20	4.6160	0.01	4.6176	0.04	
		12×12	3.0041	0.15	3.0055	0.20	
		14×14	3.0020	0.08	3.0030	0.11	
40	5	16×16	3.0006	0.03	3.0016	0.07	2.9996
		18×18	2.9998	0.01	3.0005	0.03	
		20×20	2.9998	0.01	3.0001	0.02	
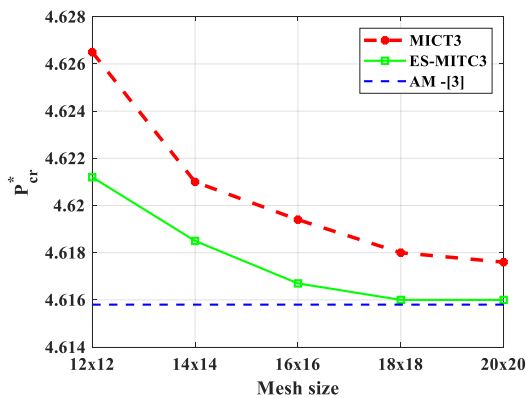
(a) The FGM plate with $a/h = 100$ and $p = 1$
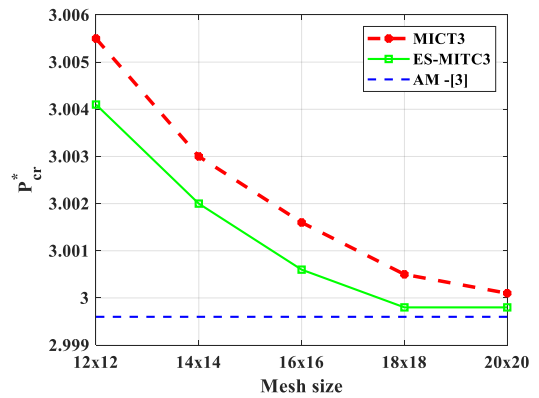
(b) The FGM plate with $a/h = 40$ and $p = 5$

Fig. 2. The convergence of mesh-size to non-dimensional critical load $P^*_{cr} = P_{cr}b^2/E_c h_0^3$ of square FGM plate

the converging results with the maximum error of 0.01% compared to those by Wu et al. [3] using the analytical method (AM). In contrast, the MITC3 element at the18x18 mesh-size has not yet converged as shown in Fig. 2. Furthermore, the obtained results by the ES-MITC3 element are compared to those of other published results as shown in Table 2. It should be noted that the error is determined by the following formula: Error (%) $= 100 \times \dfrac{|Present - [3]|}{|[3]|}$ and types of boundary conditions are defined as follows: 1) Simply supported edge boundary condition (S): $u_0 = w = \varphi_x = 0$ at $y = 0$, $y = b$ or $v_0 = w = \varphi_y = 0$ at $x = 0$, $x = a$; and 2) Clamped edge boundary condition (C): at $y = 0$, $y = b$ or $v_0 = w = \varphi_x = \varphi_y = 0$ at $x = 0$, $x = a$.

Table 2. Comparison of non-dimensional critical load $P_{cr}^* = P_{cr}b^2/E_c h_0^3$ of rectangular FGM plates. ($h = a/40; a = 1$ is fixed)

b/a	p	Wu [3]	MITC3	Error (%)	Present	Error (%)
1.5	0	11.8516	11.8913	0.33	11.8633	0.10
2	0	17.5299	17.5686	0.22	17.5481	0.10
3	0	35.1239	35.2168	0.26	35.1530	0.08
1.5	2	4.6400	4.6334	0.14	4.6430	0.06
2	2	6.8581	6.8446	0.20	6.8498	0.12
3	2	13.7697	13.7203	0.36	13.7538	0.12

Example 2. Secondly, a simply supported (SSSS) isotropic plate with linearly variable thickness $h = h_0(1 + \alpha \dfrac{y}{b})$ is considered. The non-dimensional critical load is calculated by $P_{cr}^* = P_{cr}b^2/(\pi^2 D)$ with $D = E h_0^3/12$. The obtained results of the present work are

Table 3. Comparison of non-dimensional critical load P_{cr}^* of SSSS isotropic plates with variable thickness

a/b	Method	α				
		0.125	0.25	0.5	0.75	1
	IGA-FSDT [22]	7.4621	8.7531	11.5687	14.6953	18.1368
0.5	Kantorovich method [11]	7.4645	8.7633	11.6112	14.7942	18.3175
	ES-MITC3	7.4625	8.7601	11.5989	16.6987	18.2981
	IGA-FSDT [22]	5.4194	6.3869	8.5627	11.0657	13.9017
0.7	Kantorovich method [11]	5.4199	6.3891	8.5741	11.0979	13.9730
	ES-MITC3	5.4198	6.3885	8.5738	11.0889	13.9865
	IGA-FSDT [22]	4.8428	5.7224	7.7327	10.0858	12.7877
0.9	Kantorovich method [11]	4.8413	5.7165	7.7111	10.0460	12.7381
	ES-MITC3	4.8418	5.7203	7.7198	10.0683	12.7524

compared to those by Thien et al. [22] using the IGA based on FSDT and Eisenberger et al. [11] employed Kantorovich method. These results are listed in Table 3. It is observed that the obtained results by the proposed method are in a good agreement with those published in the literature. From the above two examples, it can be concluded that the proposed method is reliable for further analyses.

4. BUCKLING ANALYSIS OF FGM VARIABLE-THICKNESS PLATES

In this section, we consider the FGM variable-thickness plate ($\frac{a}{h_0} = 100$, a is fixed) as shown in Fig. 3. The plate thickness varies along the x-direction following the law $h = h(x) = h_0(1 + \frac{x}{a})$. The material parameters of the FGM plate are given by: metal (Al) $E_m = 70$ GPa, $v_m = 0.3$ and ceramic (Al$_2$O$_3$) $E_c = 380$ GPa, $v_c = 0.3$. The non-dimensional critical load is introduced by $P_{cr}^* = \frac{P_{cr}b^2}{E_c h_0^3}$.
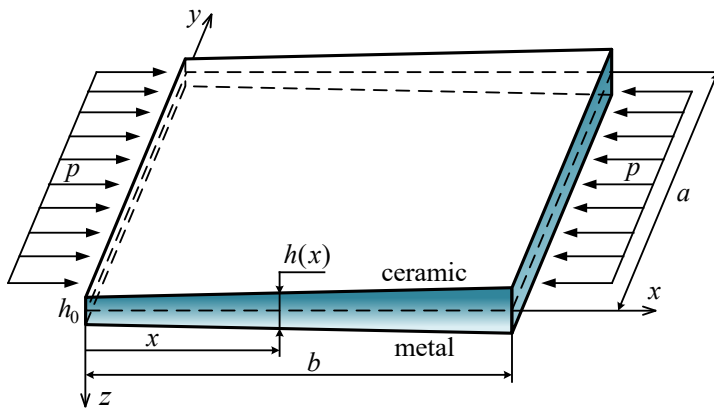
Fig. 3. The FGM variable-thickness plate under in-plane force along the x-direction

4.1. Effect of power-law index p

In order to study the effect of the power-law index p on buckling of FGM plates, we consider a square FGM plate with different boundary conditions (BCs), and the power-law index p is changed from 0 to 100. The non-dimensional critical load of the FGM plates is listed in Table 4 and displayed in Fig. 4. It can be seen that the critical force of the plate depends not only on the BC but also on the power-law index p. The rich ceramic FGM plates have a higher hardness than the rich metal FGM plates, so the critical force is higher. The critical force decreases when the power-law index p increases, and the rate decreases faster when the index p increases from 0 to 1, and slower when $p > 1$.

Table 4. The critical load of the square FGM variable-thickness plate

p	Non-dimensional critical load P_{cr}^*			
	SSSS	SCSC	CSCS	CCCC
0	5.3508	10.2158	9.2422	13.7967
0.5	3.4769	6.6299	6.0142	8.9559
1	2.6790	5.1048	4.6375	6.8965
2	2.0941	3.9872	3.6267	5.3866
5	1.7712	3.3705	3.0662	4.5523
10	1.6119	3.0683	2.7881	4.1432
20	1.4231	2.7110	2.4598	3.6605
50	1.2109	2.3091	2.0921	3.1180
100	1.1115	2.1208	1.9202	2.8639
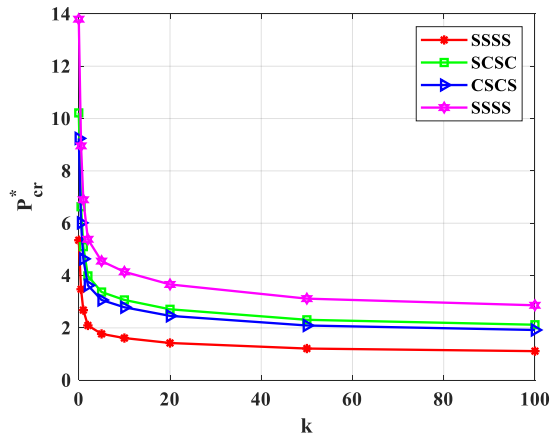
Fig. 4. The effect of p on the critical buckling load of the FGM plate
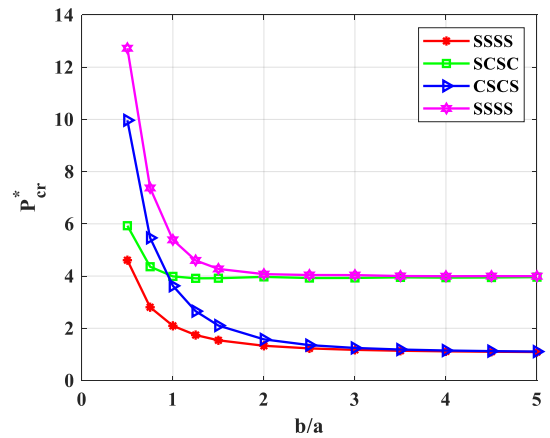
Fig. 5. The effect of b/a ratio on the critical bucking load of the FGM plate

4.2. Effect of length to width ratio b/a

Next, a rectangular FGM plate with the power-law index $p = 2$ and different BCs are considered. The length to width ratio b/a is taken from 0.5 to 5 while the width of the plate a is assumed to be constant. The non-dimensional critical loads are provided in Table 5 and presented in Fig. 5. It can be seen that the length to width ratio b/a strongly alters the critical load of the FGM variable-thickness plate. Specifically, as ratio b/a increases, the critical load decreases rapidly. Moreover, Tables 4, 5 and Figs. 4, 5 show that the fully clamped FGM plate has the greatest critical force, while the critical force is smallest in the case of the fully simple support. This is easy to understand because the fully clamped plate leads to an increase in the stiffness of the FGM plate.

Table 5. The critical load of the rectangular FGM variable-thickness plate

b/a	Non-dimensional critical load P_{cr}^*			
	SSSS	SCSC	CSCS	CCCC
0.5	4.6069	5.9284	9.9667	12.7251
0.75	2.8052	4.3575	5.4623	7.3740
1	2.0941	3.9872	3.6267	5.3866
1.25	1.7405	3.9128	2.6550	4.5983
1.5	1.5390	3.9177	2.1039	4.2724
2	1.3298	3.9678	1.5757	4.0732
2.5	1.2291	3.9242	1.3547	4.0396
3	1.1731	3.9275	1.2459	4.0361
3.5	1.1389	3.9495	1.1854	4.0006
4	1.1165	3.9389	1.1485	3.9941
4.5	1.1010	3.9441	1.1243	3.9976
5	1.0899	3.9576	1.1077	3.9947

4.3. Buckling of FGM plates with different kinds of variable-thickness

Finally, a square FGM plate with three cases of variable-thickness and power-law index $p = 2$ is considered. The plate is subjected to the in-plane compression load in the x-direction.

Case 1: linear variable-thickness $h = h(x) = h_0 \left(1 + \dfrac{x}{a}\right)$.

Case 2: parabolic variable-thickness $h = h(x) = h_0 \left(1 + \left(\dfrac{x}{a}\right)^2\right)$.

Case 3: exponential variable-thickness $h = h(x) = h_0 2^{x/a}$.

The non-dimensional critical load of the FGM plate for 3 cases are shown in Table 6.

Table 6. The non-dimensional critical load of the FGM variable-thickness plate

h	Non-dimensional critical load P_{cr}^*			
	SSSS	SCSC	CSCS	CCCC
$h = h_0 \left(1 + \dfrac{x}{a}\right)$	2.0941	3.9872	3.6267	5.3866
$h = h_0 \left(1 + \left(\dfrac{x}{a}\right)^2\right)$	1.4054	2.7527	2.3635	3.5510
$h = h_0 2^{x/a}$	1.8426	3.5406	3.1694	4.7162

The first six buckling mode-shapes of fully clamped FGM variable-thickness plates are shown in Figs. 6, 7, and 8. It can be seen that the law of thickness variation has a significant influence on the critical force and the buckling mode-shapes of plates. In these

figures, the mode-shape of buckling of the FGM variable-thickness plate is not symmetric because the thickness at each position on the plate is different. The maximum values of mode-shapes are traveled toward a smaller thickness.
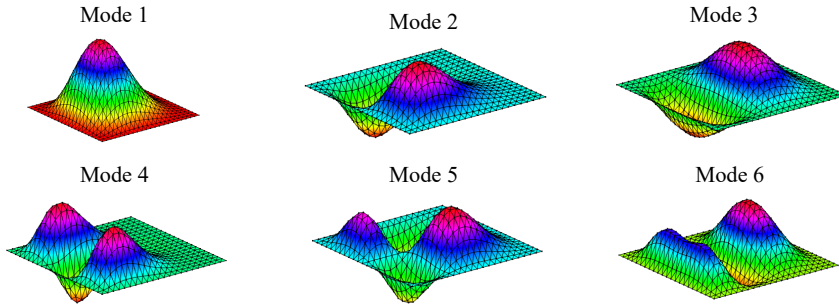
Fig. 6. The first six buckling mode-shapes of the plate with linear variable thickness
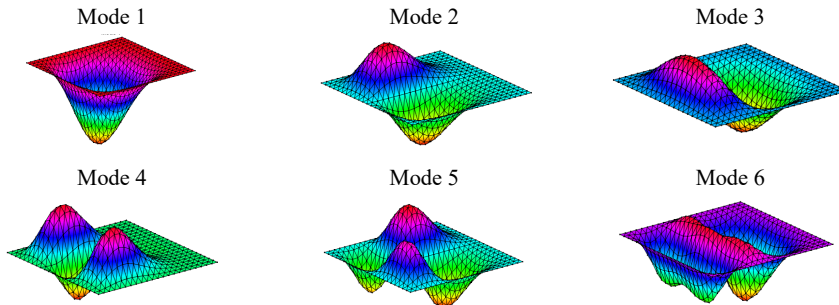
Fig. 7. The first six buckling mode-shapes of the plate with parabolic variable thickness
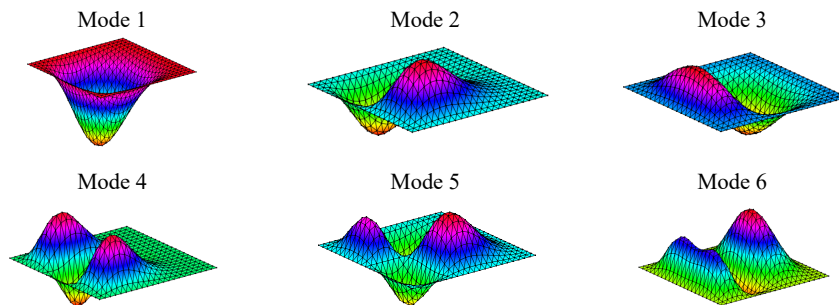
Fig. 8. The first six buckling mode-shapes of the plate with exponential variable thickness

5. CONCLUSIONS

The paper aims to extend the ES-MITC3 element for the buckling analysis of the FGM variable-thickness plates subjected to mechanical loads. The formulation is based on the FSDT due to its simplicity and computational efficiency. In the numerical examples,

the effect of geometrical parameters, material properties, boundary conditions, and the law of thickness variation to buckling of FGM plates are also examined. Through the formulation and numerical results, some main conclusions are drawn as follows:

- The results by the ES-MITC3 element are in a good agreement compared to the results in the references.

- The results by the ES-MITC3 element are more accurate and converge faster than those of the MITC3 element for analyzing variable-thickness plates. It is because the strain domains of ES-MITC3 element are smoothed and continuous over the smoothing domains, while the strain of MITC3 element on the same domains are discontinuous along the edges of elements.

- The increase of power-law index p leads to the reduction of the stiffness of FGM plates.

- Geometric parameters, boundary conditions significantly affect the buckling of the FGM variable-thickness plates.

- Using the ES-MITC3 element based on the FSDT is only suitable for thin and medium plate analysis. For thick plates, the ES-MITC3 element in the combination with the HSDT is recommended.

- The obtained numerical results are expected to be useful for the calculation and design of FGM variable-thickness plates in the future.

ACKNOWLEDGEMENTS

REFERENCES

[1] I. Ramu and S. C. Mohanty. Buckling analysis of rectangular functionally graded material plates under uniaxial and biaxial compression load. *Procedia Engineering*, **86**, (2014), pp. 748–757. https://doi.org/10.1016/j.proeng.2014.11.094.

[2] R. Saha and P. R. Maiti. Buckling of simply supported FGM plates under uniaxial load. *International Journal of Civil & Structural Engineering*, **2**, (4), (2012), pp. 1035–1050.

[3] T.-L. Wu, K. K. Shukla, and J. H. Huang. Post-buckling analysis of functionally graded rectangular plates. *Composite Structures*, **81**, (2007), pp. 1–10. https://doi.org/10.1016/j.compstruct.2005.08.026.

[4] R. Javaheri and M. R. Eslami. Buckling of functionally graded plates under in-plane compressive loading. *Journal of Applied Mathematics and Mechanics*, **82**, (2002). https://doi.org/10.1002/1521-4001(200204)82:4¡277::aid-zamm277¿3.0.co;2-y.

[5] A. M. Zenkour. A comprehensive analysis of functionally graded sandwich plates: Part 2—Buckling and free vibration. *International Journal of Solids and Structures*, **42**, (2005), pp. 5243–5258. https://doi.org/10.1016/j.ijsolstr.2005.02.016.

[6] B. A. S. Shariat and M. R. Eslami. Buckling of thick functionally graded plates under mechanical and thermal loads. *Composite Structures*, **78**, (2007), pp. 433–439. https://doi.org/10.1016/j.compstruct.2005.11.001.

[7] H.-T. Thai and D.-H. Choi. An efficient and simple refined theory for buckling analysis of functionally graded plates. *Applied Mathematical Modelling*, **36**, (2012), pp. 1008–1022. https://doi.org/10.1016/j.apm.2011.07.062.

[8] B. S. Reddy, J. S. Kumar, C. E. Reddy, and K. V. K. Reddy. Buckling analysis of functionally graded material plates using higher order shear deformation theory. *Journal of Composites*, **2013**, (2013), pp. 1–12. https://doi.org/10.1155/2013/808764.

[9] T. I. Thinh, T. M. Tu, T. H. Quoc, and N. V. Long. Vibration and buckling analysis of functionally graded plates using new eight-unknown higher order shear deformation theory. *Latin American Journal of Solids and Structures*, **13**, (2016), pp. 456–477. https://doi.org/10.1590/1679-78252522.

[10] P.-T. Thang, T. Nguyen-Thoi, and J. Lee. Closed-form expression for nonlinear analysis of imperfect sigmoid-FGM plates with variable thickness resting on elastic medium. *Composite Structures*, **143**, (2016), pp. 143–150. https://doi.org/10.1016/j.compstruct.2016.02.002.

[11] M. Eisenberger and A. Alexandrov. Buckling loads of variable thickness thin isotropic plates. *Thin-Walled Structures*, **41**, (2003), pp. 871–889. https://doi.org/10.1016/s0263-8231(03)00027-2.

[12] M. H. Naei, A. Masoumi, and A. Shamekhi. Buckling analysis of circular functionally graded material plate having variable thickness under uniform compression by finite-element method. *Proceedings of the Institution of Mechanical Engineers, Part C: Journal of Mechanical Engineering Science*, **221**, (2007), pp. 1241–1247. https://doi.org/10.1243/09544062jmes636.

[13] S. K. Jalali, M. H. Naei, and A. Poorsolhjouy. Thermal stability analysis of circular functionally graded sandwich plates of variable thickness using pseudo-spectral method. *Materials & Design*, **31**, (2010), pp. 4755–4763. https://doi.org/10.1016/j.matdes.2010.05.009.

[14] M. M. Alipour and M. Shariyat. Semi-analytical buckling analysis of heterogeneous variable thickness viscoelastic circular plates on elastic foundations. *Mechanics Research Communications*, **38**, (2011), pp. 594–601. https://doi.org/10.1016/j.mechrescom.2011.09.001.

[15] M. M. Alipour and M. Shariyat. Semianalytical Solution for Buckling Analysis of Variable Thickness Two-Directional Functionally Graded Circular Plates with Nonuniform Elastic Foundations. *Journal of Engineering Mechanics*, **139**, (2013), pp. 664–676. https://doi.org/10.1061/(asce)em.1943-7889.0000522.

[16] F. Alinaghizadeh and M. Shariati. Buckling Analysis of Variable Thickness Radially Functionally Graded Annular Sector Plates Resting on Two-Parameter Elastic Foundations by the GDQ Method. *International Journal of Applied Mechanics*, **07**, (2015). https://doi.org/10.1142/s1758825115500830.

[17] O. Bouguenina, K. Belakhdar, A. Tounsi, and E. A. Adda Bedia. Numerical analysis of FGM plates with variable thickness subjected to thermal buckling. *Steel and Composite Structures*, **19**, (3), (2015), pp. 679–695. https://doi.org/10.12989/scs.2015.19.3.679.

[18] F. Benlahcen and K. Belakhdar. Thermal buckling resistance of simply supported FGM plates with parabolic-concave thickness variation. *Steel and Composite Structures*, **29**, (5), (2018), pp. 591–602. https://doi.org/10.12989/scs.2018.29.5.591.

[19] P. P. Minh and N. D. Duc. The effect of cracks on the stability of the functionally graded plates with variable-thickness using HSDT and phase-field theory. *Composites Part B: Engineering*, **175**, (2019). https://doi.org/10.1016/j.compositesb.2019.107086.

[20] A. M. Zenkour. Bending of thin rectangular plates with variable-thickness in a hygrothermal environment. *Thin-Walled Structures*, **123**, (2018), pp. 333–340. https://doi.org/10.1016/j.tws.2017.11.038.

[21] M. N. M. Allam, R. Tantawy, and A. M. Zenkour. Thermoelastic stresses in functionally graded rotating annular disks with variable thickness. *Journal of Theoretical and Applied Mechanics*, (2018). https://doi.org/10.15632/jtam-pl.56.4.1029.

[22] T. Banh-Thien, H. Dang-Trung, L. Le-Anh, V. Ho-Huu, and T. Nguyen-Thoi. Buckling analysis of non-uniform thickness nanoplates in an elastic medium using the isogeometric analysis. *Composite Structures*, **162**, (2017), pp. 182–193. https://doi.org/10.1016/j.compstruct.2016.11.092.

[23] P.-S. Lee and K.-J. Bathe. Development of MITC isotropic triangular shell finite elements. *Computers & Structures*, **82**, (2004), pp. 945–962. https://doi.org/10.1016/j.compstruc.2004.02.004.

[24] G. R. Liu, T. Nguyen-Thoi, and K. Y. Lam. An edge-based smoothed finite element method (ES-FEM) for static, free and forced vibration analyses of solids. *Journal of Sound and Vibration*, **320**, (2009), pp. 1100–1130. https://doi.org/10.1016/j.jsv.2008.08.027.

[25] T. Chau-Dinh, Q. Nguyen-Duy, and H. Nguyen-Xuan. Improvement on MITC3 plate finite element using edge-based strain smoothing enhancement for plate analysis. *Acta Mechanica*, **228**, (2017), pp. 2141–2163. https://doi.org/10.1007/s00707-017-1818-3.

[26] T.-K. Nguyen, V.-H. Nguyen, T. Chau-Dinh, T. P. Vo, and H. Nguyen-Xuan. Static and vibration analysis of isotropic and functionally graded sandwich plates using an edge-based MITC3 finite elements. *Composites Part B: Engineering*, **107**, (2016), pp. 162–173. https://doi.org/10.1016/j.compositesb.2016.09.058.

[27] Q.-H. Pham, T.-V. Tran, T.-D. Pham, and D.-H. Phan. An Edge-Based Smoothed MITC3 (ES-MITC3) Shell Finite Element in Laminated Composite Shell Structures Analysis. *International Journal of Computational Methods*, **15**, (2018). https://doi.org/10.1142/s0219876218500603.

[28] Q.-H. Pham, T.-D. Pham, Q. V. Trinh, and D.-H. Phan. Geometrically nonlinear analysis of functionally graded shells using an edge-based smoothed MITC3 (ES-MITC3) finite elements. *Engineering with Computers*, **36**, (3), (2020), pp. 1069–1082. https://doi.org/10.1007/s00366-019-00750-z.

[29] D. Pham-Tien, H. Pham-Quoc, V. Tran-The, T. Vu-Khac, and N. Nguyen-Van. Transient Analysis of Laminated Composite Shells Using an Edge-Based Smoothed Finite Element Method. In *Proceedings of the International Conference on Advances in Computational Mechanics 2017*, Springer Singapore, (2018), pp. 1075–1094, https://doi.org/10.1007/978-981-10-7149-2_75.

[30] T. T. Tran, Q.-H. Pham, and T. Nguyen-Thoi. An Edge-Based Smoothed Finite Element for Free Vibration Analysis of Functionally Graded Porous (FGP) Plates on Elastic Foundation Taking into Mass (EFTIM). *Mathematical Problems in Engineering*, **2020**, (2020), pp. 1–17. https://doi.org/10.1155/2020/8278743.

[31] K.-U. Bletzinger, M. Bischoff, and E. Ramm. A unified approach for shear-locking-free triangular and rectangular shell finite elements. *Computers & Structures*, **75**, (2000), pp. 321–334. https://doi.org/10.1016/s0045-7949(99)00140-6.

[32] T. Nguyen-Thoi, P. Phung-Van, H. Nguyen-Xuan, and C. Thai-Hoang. A cell-based smoothed discrete shear gap method using triangular elements for static and free vibration analyses of Reissner-Mindlin plates. *International Journal for Numerical Methods in Engineering*, **91**, (2012), pp. 705–741. https://doi.org/10.1002/nme.4289.

[33] K.-J. Bathe and E. N. Dvorkin. A formulation of general shell elements—the use of mixed interpolation of tensorial components. *International Journal for Numerical Methods in Engineering*, **22**, (1986), pp. 697–722. https://doi.org/10.1002/nme.1620220312.